METHODICAL ALTERNATIVES TO THE GLACIER MOTION MEASUREMENT FROM DIFFERENTIAL SAR INTERFEROMETRY

A.I. Sharov [a], K.Gutjahr [a], F. Meyer [b], M. Schardt [a]

[a] Institute of Digital Image Processing, Joanneum Research, Graz, Austria - (aleksey.sharov, karlheinz.gutjahr)@joanneum.at
[b] Chair for Photogrammetry and Remote Sensing, Technical University Munich, Germany - franz.meyer@bv.tu-muenchen.de

Commission III, WG III/3

Key words: Differential SAR Interferometry, Phase Gradient, Glacier Motion, Velocity, Geodetic Survey

ABSTRACT:

Algorithmic variations to the glacier motion estimation from differential SAR interferometry are discussed in the present paper. Two efficient albeit relatively simple algorithms for modelling glacier dynamics using spaceborne INSAR data have been devised and tested as alternatives to the conventional DINSAR approach. Neither of the algorithms involves the procedure of interferometric phase unwrapping, thus excluding the areal error propagation and improving the modelling accuracy. In general, they remain feasible even under significant phase noise. An original gradient approach (GINSAR) to differential processing of repeat-pass SAR interferograms based on the calculation of interferometric phase gradients, the generation of glacier slope maps and the analysis of differences between multitemporal slope maps provides global and fast solutions to unsupervised glacier change detection and ice motion estimation. A transferential approach is based on the interferometric measurement of the fast-ice translation forced by the glacier flow and provides good reference values on the glacier frontal velocity and velocity gradients for the GINSAR technique. A comparative analysis of the results obtained by different techniques was performed and algorithmic singularities were discussed. The revealed differences of up to 40% between the GINSAR velocities and those surveyed in the field are explained.

1. PRELIMINARY REMARKS

The high level of scientific and industrial interest in satellite radar interferometry (INSAR) has not been extinguished over the past 10 years. The INSAR method is greatly valued by experts studying glacier dynamics, because of its notable data availability and astonishing sensitivity to ice motion / deformation. Spectacular results using multitemporal repeat-pass interferograms from ERS-1/2 and RADARSAT satellites for glacier-flow measurement, strain rate estimation and detection of rapid glacier changes are reported every year (Bamler & Hartl, 1998; Forster et al., 1999; Rabus & Fatland, 2000)

Differential interferometry (DINSAR), the methodological variant based on differencing between two SAR interferograms obtained at different times over the same glacier, became especially popular among glaciologists investigating glacier mass flux and mass balance. Although the theory of conventional DINSAR is well established (Gabriel et al., 1989; Joughin et al., 1996), the technological perfection in converting differential SAR interferograms to a surface-velocity vector field has yet to be completed. There are several approaches to solving the principal task of differential interferometry, i.e. distinguishing between the impacts of surface topography and surface displacement on the interferometric phase. A concise classification and characterisation of algorithmic variations to differential interferometric processing of SAR imagery can be found in (Wegmüller & Strozzi, 1998).

Generally speaking, all known DINSAR algorithms are based on practically the same complement of operations including co-registration of interferograms, phase scaling and subtraction and, inevitably, the procedure of interferometric phase unwrapping; the latter is reputed to be the most sophisticated and problematic calculus in interferometric signal processing. Apart from the algorithmic complexity and computational load, this integral procedure is error-prone and frequently becomes impossible, at least locally, because of complex glacier topography and significant phase noise at glacier fronts, walls

and tops. Moreover, in conventional DINSAR the operation of phase integration has to be performed twice, i.e. in each of two original interferograms. This leads to error propagation. In our experience, none of the available phase-unwrapping algorithms such as branch-cut, least squares or minimum-cost flow techniques, provide reliable and detailed surface models of test glaciers, even if high-quality interferograms are used. The procedure of phase unwrapping is currently reputed by experts to be a break-point in the INSAR technology; the quality of consecutive products cannot be guaranteed (H.Raggam, personal communication 2002).

Our recent research has thus been focused on designing and testing alternative algorithms for glacier motion estimation and variational analysis of ice velocities without phase unwrapping. Several alternative algorithms using

- transferential approach to the ice motion interpretation in single interferograms and
- gradient approach to the glacier surface modelling and glacier velocity measurement

were developed and tested using the ERS-1/2-INSAR data obtained over large tidewater glaciers in the European Arctic.

The present paper describes these new algorithms and their singularities, and provides the most interesting results of tests and validations. The tachometric accuracy was verified by mutual comparison of models obtained by alternative techniques and compared with results of geodetic observations from the field campaign 2001.

2. STANDARD DINSAR TECHNIQUE FOR THE GLACIER MOTION ESTIMATION AND ITS LIMITATIONS

Compared to other remote sensing techniques, the DINSAR method has the one wonderful advantage: it allows quite small glacier changes / motions in the centimetre range to be detected and measured from satellite SAR images with a nominal ground resolution of several tens of meters. A full separation between

the impacts of glacier topography and glacier motion on the interferometric phase is a prerequisite for attaining such a high performance.

Although the non-linear behaviour of the SAR interferometer with regard to the phase may not be excluded, especially when it comes to INSAR modelling of active glaciers, for the sake of simplicity, the unwrapped interferometric phase is usually treated as a linear combination of several phase terms. For example, in (Bamler & Hartl, 1998), the interferometric phase is presented as a sum of independent contributions from imaging geometry (the flat earth phase) ϕ_o, topography ϕ_{topo}, glacier flow ϕ_{mot}, atmospheric disturbances ϕ_{atm} and noise ϕ_{noise}

$$\phi = \phi_o + \phi_{topo} + \phi_{mot} + \phi_{atm} + \phi_{noise} . \qquad (1)$$

The proper selection of interferometric pairs allows the terms ϕ_{atm} and ϕ_{noise} to be kept small (Sharov & Gutjahr 2002), and, after the flat earth correction is performed, the equation (1) can be rewritten as a function of only the topographic phase and the motion phase

$$\varphi \cong \frac{4\pi}{\lambda} \cdot \left(\frac{B_\perp \cdot h}{R \cdot \sin\theta} + V \cdot T \right) , \qquad (2)$$

where φ denotes the interferometric phase after the flat-terrain phase correction; λ is the wavelength of SAR signal, $B_\perp$ is the perpendicular component of the spatial baseline, R - the slant range, θ - the look angle, V - the projection of the flow vector on the line-of-sight direction, and T is the temporal baseline.

Theoretically, the isolation of the motion phase from the topographic phase can be performed by differencing between two SAR interferograms of the same glacier, one of which does not contain the phase term related to the ice motion. In practice, however, it is nearly impossible to find out the real interferometric model of a living glacier without motion fringes. This holds good especially for the study of fast-moving polar glaciers, such as large tidewater glaciers. Their velocities reach tens of centimetres a day and more. Thus, in general, glaciologists must deal with a pair of SAR interferograms, each containing both topographic and motion phases.

Interferograms in processing have different spatial baselines. Therefore, one of the interferograms must be scaled before the subtraction in order to account for different surveying geometry and to compensate the topographic phase. The procedure of scaling is usually applied to the unwrapped phase picture because scaling of the wrapped phase provides reasonable results only for integer scaling factors (Wegmüller & Strozzi 1998). After phase unwrapping and co-registering both pictures can be combined and subtracted one from the other. This is generally considered to be a somewhat complicated technique, since it involves up to ten obligatory processing steps. Furthermore there are several major limitations to conventional DINSAR impeding its application to glacier motion estimation.

In the differential interferogram, the topographic phase is compensated and the equation for differential phase is given as follows

$$\varphi_d \cong \frac{4\pi}{\lambda} \cdot \left(V_1 \cdot T_1 - \frac{B_{\perp 1}}{B_{\perp 2}} \cdot V_2 \cdot T_2 \right) . \qquad (3)$$

From the equation (3) it is seen that the motion phase $\phi_{mot\,2}$ is also scaled, and the direct estimation of the glacier motion is still impossible because only the difference between two motion phases is given. The proper selection of interferograms with different temporal baselines $T_1 \neq T_2$ does not help much in this case because of the decorrelation noise that increases drastically with time between surveys. Practically, only SAR interferograms with a temporal interval of 1 day and 3 days can be applied to glacier modelling.

The simplest way to solve the equation (3) with regard to the velocity V_1 or V_2 is to assume that the glacier velocity remains constant over the time span covered by both interferograms, i.e. $V_1 = V_2 = V$. Although applicable to modelling in the accumulation area of large ice domes, the stationary flow assumption has often proved to be incorrect in fast moving areas of outlet glaciers (Fatland & Lingle, 1998). A more reliable constraint has been offered in (Meyer & Hellwich, 2001), who supposed that the velocity ratio V_1/V_2 remains constant over the whole glacier area. Still, the validity of such an assumption has not been confirmed empirically.

Another serious limitation to DINSAR is that only the velocity component in satellite look direction can be derived from differential SAR interferograms. Hence, some additional constraints are necessary for estimating the horizontal and vertical components of the ice-velocity vector. A common way to proceed is to assume that the glacier flow is parallel to the ice surface, normal to topographic contours and parallel to glacier walls. The surface parallel flow assumption is considered to be more or less realistic when the surface-normal velocity is small, which is the case only over some parts, e.g. around the equilibrium line, of a valley glacier (Rabus & Fatland 2000).

Sometimes, a combination of three or more interferograms taken either from parallel or from opposite, i.e. ascending and descending orbits is used, but the necessity of performing two-dimensional phase unwrapping of each original interferogram in the case of phase noise with unavoidable error propagation is probably the most serious restriction to the multiple baseline approach in particular and to the whole DINSAR method in general. An essential enhancement to the multiple baseline technique based on stacking / averaging phase gradients was offered in (Sandwell & Price 1998) with the aim to decrease errors due to atmospheric-ionospheric disturbances and to improve the general quality of INSAR data for both topographic recovery and change detection. The phase gradient approach ensures serious processional advantages, e.g. it delays the procedure of phase unwrapping until the final step of the DINSAR processing, but remains, however, largely untested and is rarely mentioned in literature.

3. ALGORITHMIC ALTERNATIVES TO DINSAR MODELLING OF GLACIER DYNAMICS

As has been seen, obtaining several suitable INSAR pairs and their differential processing for studying glacier dynamics, is not an easy matter in the first place. There is thus a natural desire to try simpler techniques that do not involve complex process artifices such as phase unwrapping and do not require additional topographic reference models.

If the length of the interferential baseline is, by lucky chance, very short (several meters), then the glacier motion can be determined directly in a single interferogram and there is no

need for the DINSAR approach at all. Sometimes, essential ice flow is recorded in relatively flat glacier areas. If the interferential baseline is not long (several tens of meters), the topographic phase vanishes in such areas, and the glacier motion also can be evaluated (locally) from a single SAR interferogram. From a practical point of view, however, such cases should be treated as an exception to the rule, and we thus applied such interferograms to the verification of results obtained by other DINSAR techniques. In the next chapter, we present an original and simple approach to measuring frontal velocities of tidewater glaciers from single SAR interferograms.

3.1 Transferential approach

For most tidewater glaciers, the longitudinal strain rate and the ice velocity attain their maximum at the glacier front. There are many crevasses at the front part of the glacier tongue, the surface is very rough and the block-wise ice motion is incoherent (Forster et al., 1999). Both, the amplitude and the coherence of the interferometric signal from the glacier surface is usually quite low near the glacier face, and the interferential picture of glacier exteriors is characterised by poor quality. This explains why reports on using INSAR data for the measurement of frontal glacier velocities are quite few in number.

In contrast to the glacier surface, the area of fast sea ice attached to the glacier face is often reproduced with quite good coherence and demonstrates good visibility of interferential fringes. Vast plane floes of young coastal ice with a very small elevation above sea level thus represent an ideal surface for the interferometric analysis of small motions, such as translation, tilting and rotation. There is no need for topographic reference in this case. This factor makes it possible to accurately measure frontal glacier velocities in single SAR interferograms by analysing the fast-ice motion forced by the glacier flow.

In winter interferograms, the effect of lateral displacement of young coastal ice pushed by moving glacier manifests itself as a zone of concentric hemispherical or hemi-elliptical fringes converging at the tips of the glacier front (Fig. 1). Such interferential features called "outflows" are permanently found at fronts of *nearly all* active tidewater glaciers. The orientation of outflows mostly coincides with the cross-track direction that indicates the lateral character of corresponding motions. Tilting and bending of ice floes due to the atmospheric/oceanic forcing, e.g. tidal effects, would produce fringes in any orientation. Rotation produces fringes parallel to the track direction. Also regions of high deformation are characterised by high local fringe rates and increased phase noise. But usually we did not observe any significant phase noise in the area of outflows and did not detect the presence of significant deformation features (cracks, ridges) in the young sea-ice cover by jointly interpreting corresponding amplitude, coherence and fringe images. Thus, the origin of "outflows" is believed to be related primarily to the horizontal displacement of the coastal ice.

It is reasonable to assume that in the immediate proximity of the glacier face and under calm weather conditions, the local speed of the fast-ice translation is equal to the frontal velocity of gently sloping tongues of tidewater glaciers. Then, in the tide-coordinated INSAR data without significant tidal effects, the horizontal (frontal) glacier velocity in the SAR-range direction can be simply determined by counting the (real) number of interferential fringes k within the "outflow" as follows

$$V_{hr} = 0.5\lambda \cdot k \cdot (T \cdot \sin\theta \cdot \cos\beta)^{-1}, \qquad (4)$$

where $\lambda = 5.66$ cm is the wavelength, θ - the look angle measured from the vertical, β - the flow direction angle measured from the cross-track direction, and T is the temporal baseline of the interferogram.

An application of an approach of this kind known as *transferential* [from Latin transferre: *trans*-across, change + *ferre* to carry] to ERS-1/2-INSAR data processing allowed the frontal velocities of 52 large Eurasian tidewater glaciers oriented in the SAR-range direction to be determined for the first time in the history of their exploration (Sharov & Gutjahr 2002). Transverse variations of the frontal velocity along the glacier face can be evaluated by analysing the shape of outflows. The fringe rate within outflows decreases offshore and vanishes with the distance from the glacier front that corresponds to the localised and decelerated mode of displacement. The amount of displacement usually increases along the ice coast from zero at the tips of the glacier front to its maximum in the mid point at the glacier snout.

The lateral extension of an "outflow" and the number of interferometric fringes within increases with the time interval between SAR surveys, though the local fringe rate remains nearly unchanged. For example, Figure 1 shows a typical "outflow" at the front of Impetuous Glacier, Russian Arctic as shown in the interferograms generated from ERS-1/2-SAR images taken at 1 (a) and 3 (b) day intervals. The sea ice thickness grows through time and sea-ice deformation features become noticeable in late-winter interferograms, but, nevertheless, the transferential technique remains feasible up to the time of melting and disintegration of the coastal ice. The main drawback to the transferential technique is that it is not suited for the velocity measurement / representation over the whole glacier area. For the reliable separation between the topographic and the motion phase and the accurate determination of the velocity field over the whole glacier area we devised (independently of the publication by D.Sandwell & E.Price) an original gradient approach, which is presented below.
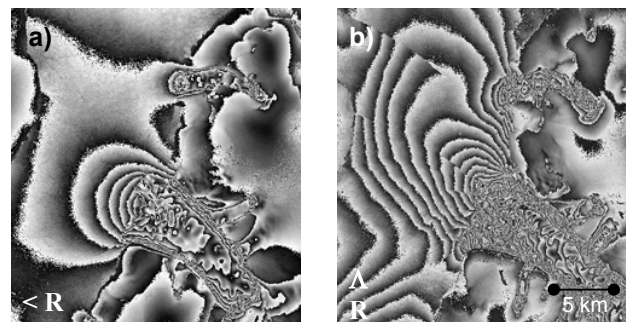

Figure 1. "Outflows" in interferograms of 17/18 December, 1995 ($B_\perp = -41$ m, a) and 23/25 February 1994 ($B_\perp = -34$ m, b)

3.2 Gradient Approach

Gradient approach to differential processing of SAR interferometric data (GINSAR) is based on the calculation of interferometric phase gradients, the generation of glacier slope maps without interferometric phase unwrapping and the analysis of differences *between slope maps* generated from multitemporal INSAR sets. The underlying concept of the GINSAR technique is to make use of the fact that, for the great majority of points in the interferential picture, partial derivatives of the wrapped interferential phase are equal to partial derivatives of the unwrapped phase, i.e.

$$\frac{\partial W\{\varphi(x,y)\}}{\partial x} = \frac{\partial \varphi(x,y)}{\partial x}, \ if \ \frac{\partial \varphi(x,y)}{\partial x} \in [-\pi, +\pi);$$

$$\frac{\partial W\{\varphi(x,y)\}}{\partial y} = \frac{\partial \varphi(x,y)}{\partial y}, \ if \ \frac{\partial \varphi(x,y)}{\partial y} \in [-\pi, +\pi), \quad (5)$$

where W denotes the wrapping operator such as that $W\{\varphi\} = \varphi + 2\pi k, \ k \in I$.

Unlike (Sandwell & Price 1998), we approximate the partial derivatives of interferometric phase in azimuth (x) and range (y) direction by differences as (Sharov & Gutjahr 2002)

$$\frac{\partial \varphi(x,y)}{\partial x} \approx \nabla \varphi_x(x,y) = \frac{\varphi(x + \Delta x, y) - \varphi(x,y)}{\Delta x};$$

$$\frac{\partial \varphi(x,y)}{\partial y} \approx \nabla \varphi_y(x,y) = \frac{\varphi(x, y + \Delta y) - \varphi(x,y)}{\Delta y}, \quad (6)$$

where the shift values Δx and Δy usually equal 1 pixel. Thus, in our practice, the partial derivative of interferometric phase is calculated by subtracting an original interferential picture from a translated version of the same interferogram. The resultant gradient picture called *topogram* (Fig. 2, a) can be directly converted to the glacier slope map without phase unwrapping. The terrestrial slope value ε is calculated on a pixel-by-pixel basis as follows

$$\cos \varepsilon = \frac{\Delta p}{\sqrt{\Delta h_x^2 + \Delta h_y^2 + \Delta p^2}}, \quad (7)$$

where Δp is the pixel diagonal size on the ground. The height increments Δh_x and Δh_y are defined as

$$\Delta h_{x,y} \cong C(x,y) \cdot \nabla \varphi_{x,y}, \quad (8)$$

where $\quad C(x,y) = 0.25\pi^{-1} \cdot \lambda \cdot B_\perp^{-1}(x) \cdot R(y) \cdot \sin \theta(y) \quad (9)$

is the conversion factor depending on the imaging geometry.

Our topograms and slope maps are represented in the form of an RGB image. In the topogram, the first two layers represent partial phase gradients $\nabla \varphi_x$ and $\nabla \varphi_y$. The third layer gives the full height increment representing the rate of increase of $h(x,y)$ per unit distance, which is defined as

$$\Delta h(x,y) = \Delta h_x \cdot \Delta x + \Delta h_y \cdot \Delta y. \quad (10)$$

The first two layers of the slope map represent the slope values in azimuth and range direction defined separately from the next equations

$$\varepsilon_x = \tan^{-1}(\Delta h_x / \Delta p_x) \quad \text{and} \quad \varepsilon_y = \tan^{-1}(\Delta h_y / \Delta p_y) \quad (11)$$

and the third layer shows the absolute slope value ε. Therefore, third layers in topograms and slope maps can be compared with the corresponding results obtained from other interferograms more or less independently of their range and azimuth direction.

Another significant advantage of the GINSAR technique is that the topogram can be scaled with any real, not necessarily integer factor, allowing for any linear combination between the topograms obtained from two different interferograms. Hence, we can easily compensate the topographic phase by differencing between two scaled and co-registered topograms. Assuming that $\nabla \varphi = \nabla \varphi_{topo} + \nabla \varphi_{mot}$ and $C_1 \cdot \nabla \varphi_{topo\,1} = C_2 \cdot \nabla \varphi_{topo\,2}$, the operation of differencing between the third layers of two topograms can be formulated as follows

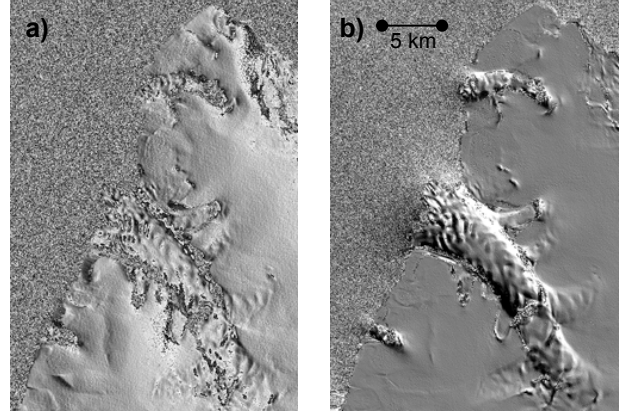$$F = C_1 \cdot \nabla \varphi_{mot\,1} - C_2 \cdot \nabla \varphi_{mot\,2}. \quad (12)$$

Figure 2. Topogram (a) and fluxogram (b) of Impetuous Glacier

The resultant picture $F(x,y)$ containing only the differential motion phase without topographic phase is called *fluxogram* (Fig. 2, b) following the definition given by I.Newton to differential calculus (*fluxions*, from Latin flüxus – flow, continual change). The fluxogram is represented in the form of a 4-layer image with the first two layers showing the difference between scaled partial motion increments in azimuth and range direction. The third layer shows the difference between full motion increments and the fourth layer gives the direction of differential motion calculated as the ratio between the first two layers. Although the fluxogram provides only the relative information about the glacier velocity, it can be directly applied to the analysis of the longitudinal strain rate σ. The latter is usually calculated as a difference between two neighbouring velocity values divided by the distance between velocity records along the longitudinal transect (Forster et al., 1999).

In order to solve the equation (12), e.g. with respect to $\nabla \varphi_{topo\,1}$, firstly, we assume that the relation between the velocity gradients $a = \nabla \varphi_{mot\,2} / \nabla \varphi_{mot\,1}$ remains constant over the whole glacier area. In contrast to the assumption made in (Meyer & Hellwich, 2001), such a constraint seems to be more reliable in the glacier environment, though it also has to be verified empirically. Secondly, we determine some reference values for $\nabla \varphi_{mot\,2}$, e.g. by analysing the frontal velocity gradients derived from winter topograms on the basis of the transferential approach. Finally, the third layer of the fluxogram is converted to a new image product using the following relation

$$\nabla \varphi_{mot\,1} = \Delta V_1 \cdot T_1 = F \cdot (C_1 - aC_2)^{-1}, \quad (13)$$

where ΔV_1 is the velocity gradient in the first interferogram. It is interesting to note that the ratio between the conversion

factors $b = C_2/C_1$ can always be treated as a constant. According to our tests, in the majority of cases, the deviation of b from the mean value did not exceed 1 percent over the whole overlap area between two different interferograms.

In order to obtain the absolute glacier velocity, the integration of velocity gradients in the output GINSAR product has yet to be performed. The absolute glacier velocity can be found by performing the line integral of its partial gradients ∇V_x and ∇V_y

$$V(x,y) = \nabla V(1,y) + \sum_{i=1}^{x-1} \nabla V_x(i,y),$$
$$V(x,y) = \nabla V(x,1) + \sum_{j=1}^{x-1} \nabla V_y(x,j) \qquad (14)$$

with the subsequent or preliminary linear (line by line) high-pass filtering and averaging of results obtained in the azimuth and range directions as offered in (Scambos & Fahnestock, 1998). Another interesting approach to the integration of velocity gradients is based on the adaptation of available algorithms for one- or two-dimensional phase unwrapping, but this method has not been tried yet.

An alternative local solution that we found useful in our study is to solve an over-determined system of linear equations in the form of

$$l + v = Ax \text{ with } v^T v = \min \qquad (15)$$

in a least-squares manner. In (14), l is the vector of observations ∇V_x and ∇V_y with the dimension of $2(n-1)^2$, v is the vector of residuals, A is the design matrix and x is the vector of unknowns. The total number of unknowns is equal to the number of pixels $u = n^2$.

In our case, the generally large matrix of normal equations $N = A^T A$ is sparse and banded with a bandwidth of n. In order to solve such a matrix, we apply the modification of the Cholesky algorithm offered in (Schuh 1998). The number of operations is then reduced to $0.5 \cdot n^4 + 3n^3 + 0.5 \cdot n^2 + 5n$. As we have only relative measurements between two pixel values, the equation system has a rank of $u - 1$, which means that one more independent measurement, e.g. one reference point with known (zero) velocity, is still necessary.

3.3 Algorithmic Singularities

It is worth noting that the basic equation (5) becomes invalid if the module of the phase difference between two neighbouring pixels in azimuth or/and in range direction exceeds π. In the interferential picture, such locations called *singularities* are related either with the phase noise or with steep topography and / or highly accelerated motion.

Apart from the phase noise influence, the module of the partial phase gradient will exceed π, if the terrestrial slope exceeds the critical value ε_{cr}, which can be determined from the following equation

$$\varepsilon_{cr} = \tan^{-1}\left(\frac{\lambda R \cdot \sin\theta}{4 B_\perp \cdot \Delta p}\right). \qquad (16)$$

The graph in Figure 3 shows, however, that depending on the length of the normal baseline and look angle (theta) the value of

critical slope is usually not smaller than 50°. Such inclinations might be excluded from consideration.
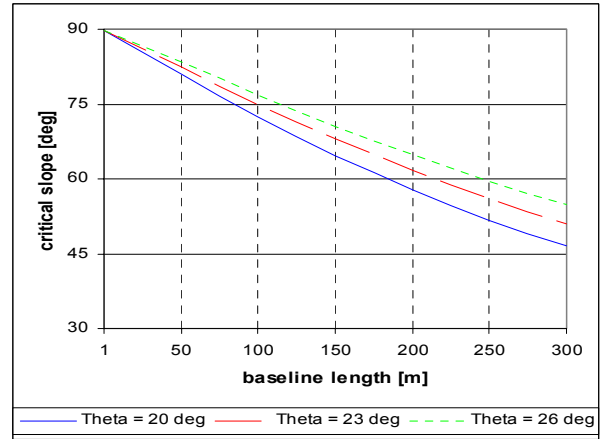

Figure 3. Critical slope versus normal baseline (ERS-1/2-SAR)

In areas of high deformation along glacier walls and at glacier fronts with numerous crevasses and non-uniform motion of ice blocks, the motion phase gradient can also exceed π, if the velocity gradient between two neighbouring pixels is larger than 0.25λ, i.e.

$$\Delta V_{cr} = V_{y+1} - V_y \geq \lambda/4 = 1.415 \, [cm/day]. \qquad (17)$$

Other kinds of singularities in the form of narrow "traces" from the edges of interferometric fringes can also be seen in topograms. Such singularities are compensated by locally adding or subtracting a value of 2π to / from the topogram as follows

$$\hat{\nabla}\varphi_{x,y} = \nabla\varphi_{x,y} + 2\pi \cdot n; \; n = \begin{cases} -1, & if \, \nabla\varphi_{x,y} \geq \pi \\ 0, & if -\pi \leq \nabla\varphi_{x,y} < \pi. \\ +1, & if \, \nabla\varphi_{x,y} < -\pi \end{cases} \quad (18)$$

A flow chart showing the sequence of principal stages of the GINSAR technique is given in Figure 4. The GINSAR algorithm has been implemented in the new RSG 4.0 software package distributed by Joanneum Research.

4. EXPERIMENTAL VERIFICATION AND FIELD VALIDATION

The efficacy and robustness of our new algorithms have been verified by several independent experts who processed multitemporal (D)INSAR data using the GINSAR technique. Up to now, 27 GINSAR models have been processed and all results were quite satisfactory. The time required for processing one differential model did not exceed 4 hours. Visual analysis confirmed the fine detail of GINSAR products and revealed that the original ground resolution of INSAR data has been nearly preserved.

The INSAR velocities of glaciers were measured several times using different interferograms and the results appeared quite consistent. The relative tachometric accuracy was verified by comparing the velocities of 7 test glaciers measured by conventional DINSAR and our alternative techniques. The mean difference between the velocities was estimated at +6.3

cm/day, and the maximum difference reached 58%. The r.m.s. difference was given as 6.34 cm/day. We understood that such a comparison could not serve as an estimate of absolute accuracy, but indicated only methodological differences.
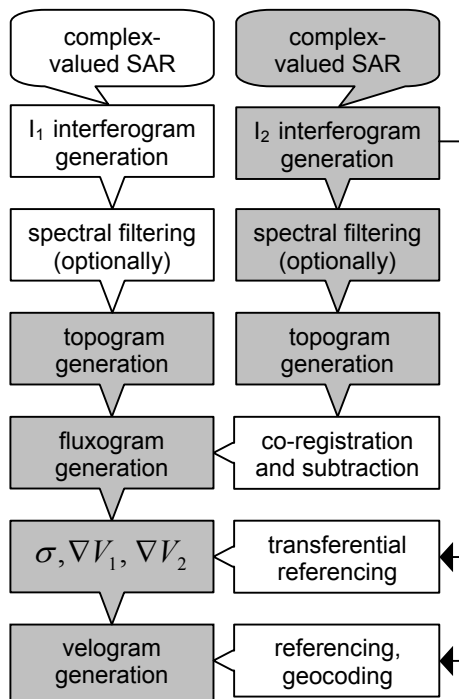

Figure 4. Principal flowchart of the GINSAR technique

Absolute tachometric validations were performed during the field work undertaken in Novaya Zemlya in September 2001, when the frontal velocities of several test tidewater glaciers were surveyed using precise geodetic equipment. Preliminary measurements of the maximum velocities were made in the lab using 4 INSAR models taken over the same glaciers in March 1996. The geodetic surveys were performed using two alternative techniques. A conventional geodetic technique of forward intersection is based on multitemporal observations of identical points at the glacier front from two different positions with a known baseline. The polar idea of a non-traditional "touch-and-go" technique is to install the laser line in a tangential position at a predefined distance from the glacier front and to frequently measure the distance to any point on the opposite coast in order to record the instant when the glacier will cross the laser line and the measured distance will change abruptly (Sharov et al., 2001). This technique made use of a LDI-3 laser rangefinder (range up to 19 km without retro-reflector) mounted on a Leica T1602 theodolite (angular accuracy 0.5 mgon). Typical results of velocity measurements are given in Table 1.

The results obtained indicate that the winter INSAR velocities are somewhat lower than those from ´summer´ geodetic surveys, which corresponds to the observations performed by other investigators in other regions (e.g. Rabus & Fatland 2000). Apart from the different duration of observations and seasonal changes in the glacier motion, this fact can be explained by the inherent influence of INSAR undersampling if velocity gradients between neighbouring pixels exceed 0.014 m/day. In spite of the revealed tachometric differences of up to 40% and more, the spatial correlation between the GINSAR velocities and those surveyed in the field was quite high over all glaciers.

Glacier	Frontal velocity [m/day]		
	INSAR	Fwd. intersection	Touch-and-go
Rykatchova No. 88	0.56	0,68±0,14	0,83±0,20
Mack No.91	0.37	0,61±0,13	0,73±0,15

Table 1. Glacier velocities measured in the lab and in the field

5. CONCLUSIONS

The global and stringent GINSAR algorithm devised for the glacier motion estimation does not involve complex process artifices and does not require additional topographic reference models thus eliminating areal error propagation, and the resultant velocity gradient values are quite tolerant of local phase errors. Therefore, such an approach remains feasible even under significant phase noise. The stage of phase filtering, which is usually included in all known phase unwrapping algorithms, becomes optional in our case and is used mostly for cosmetic reasons. The high metric quality, detail and complementary thematic contents of the GINSAR products, which are called *topogram* and *fluxogram,* show the expedience of this technique and its applicability to solving various tasks in the area of unsupervised glacier change detection and glacier mass balance measurement. The transferential approach based on the analysis of fast-ice motion forced by the glacier flow provides good reference values for the glacier frontal velocity and velocity gradients and can be considered as a complementary operation to the GINSAR method. The combination of our algorithms provides a unique opportunity to reduce the computational load and to mitigate some problems related to the operation of interferometric phase unwrapping.

References

Bamler, R., Hartl, P., 1998. Synthetic apertur radar interferometry. *Inverse Problems*, 14, R1-R54.

Fatland, D., Lingle, G., 1998. Analysis of the 1993-95 Bering Glacier surge using differential SAR interferometry. *J.Glac.,* 44 (148), pp. 532-545.

Forster, R. et al., 1999. Interferometric radar observations of Glaciares Europa and Penguin. *J.Glac.,* 45 (150), pp. 325-336.

Gabriel, A. et al., 1989. Mapping small elevation changes over large areas: differential radar interferometry. *J. Geophys.Res.*, 94, B7, pp. 9183-9191.

Joughin, I. et al., 1996. Estimation of ice-sheet motion using satellite radar interferometry. *J.Glac.,* 42 (142), pp. 564-575.

Meyer, F., Hellwich, O., 2001. Estimation of Glacier Topography and Velocity Using Correlation Minimization. Proc. of DGPF Jahrestagung Sept. 2001, Konstanz, pp. 467-474

Rabus, B.T., Fatland, D.R., 2000. Comparison of SAR-interferometric and surveyed velocities on a mountain glacier: Black Rapids Glacier. *J. Glac.,* 46 (152), pp. 119-128.

Sandwell, D., Price, E., 1998. Phase gradient approach to stacking interferograms. *J. Geophys. Res.*, 103, No. B12, 30183-30204.

Scambos T., Fahnestock, M., 1998. Improving DEMs over ice sheets using AVHRR photoclinometry *J.Glac.*, 44(146), pp.97-103.

Sharov, A.I., Gutjahr K., 2002. Some methodological enhancements to INSAR surveying of polar ice caps. In: Observing our environment from space. Proc. of the 21st EARSeL Symp, pp.65-72.

Sharov, A.I. et al., 2001. Results of the field campaign in Barents and Kara seas on board the Hydrologist ship. In: Annual scientific report to the INCO Commission, P 9, pp.1-20.

Wegmüller U., Strozzi T., 1998. Characterization of differential interferometry approaches. In: Proc. EUSAR'98, Berlin, p.237-240.